Noise Properties and Phase Resolution of Interferometer Systems Interrogated by Narrowband Fiber ASE Sources

Hyo Sang Kim, Ronald P. H. Haaksman, Trevor P. Newson, and David J. Richardson

***Abstract*— We present the results of a detailed theoretical and experimental study of the noise properties of various interferometer systems interrogated using narrowband spontaneous emission. The filtering effect of the interferometer is shown to introduce periodic structure in the optical noise spectrum with a period, level, and modulation depth that depends on the exact interferometer configuration and implementation, as well as the source linewidth and spectral shape. Our theoretical analysis, based on the assumption of a Gaussian random process model for the inherent source noise is in good agreement with our experimental results. Finally, using a dual Mach–Zehnder interferometer incorporating a frequency shifter, we show that minimum phase sensitivities of a few tens of μrad/$\sqrt{\text{Hz}}$ can be achieved for practical values of length mismatch by optimization of the source linewidth, heterodyne frequency, and interferometer birefringence. We believe the approach to be suitable for a broad range of sensing applications.**

***Index Terms*—ASE source, fiber-optic acoustic sensor, interferometer, optical fiber sensor, optical source noise.**

I. Introduction

DURING the past ten years, tremendous advances have been made in the development of rare-earth-doped fiber fabrication and associated semiconductor pump laser technology. The advances have been driven by the need for efficient, high-performance amplifiers within the telecommunications industry, but have resulted in the parallel development of a range of high-performance fiber laser systems with applications across an extended range of market sectors. Fiber-based amplified spontaneous emission (ASE) sources are one such example offering high optical powers (>10 dBm) over broad spectral bandwidths (>40 nm). Such sources have potential telecommunication applications, for example when spectrally sliced they can be used for a range of WDM transmission applications where crosstalk and nonlinearity are a key issue [1]. However, their use is common in the optical sensing field where they are an established tool for interrogating fiber-based sensors such as fiber-optic gyroscopes [2] and fiber Bragg grating (FBG)-based systems [3].

The coherence properties of spectrally filtered, narrowband ASE sources make them attractive for use with interferometric sensor arrays. The performance of sensor interrogation systems based on the coherence multiplexing method and conventional laser sources [4], [5] is limited by phase induced intensity noise [6], [7]. This limitation can be eliminated by the use of appropriate optical gating, and good sensitivity has been achieved [8]. However, imperfect switching, coupled to the inevitable switching speed limitations, can cause problems due to crosstalk between channels and can give rise to signal processing difficulties, alternative approaches are therefore of great interest.

In principle, the use of a broad-band (>20 nm bandwidth) source such as a superluminescent diode (SLD) or a fiber ASE source can enhance the inherent sensitivity of a coherence multiplexed system and provides improved resistance to crosstalk effects. However, this is not a practical solution for an extended fiber-based system (e.g., an acoustic sensor system, where sensor length is required to obtain sufficient acoustic sensitivity), since in order to obtain the required level of visibility length matching within the interferometer needs to be obtained to within the coherence length of the optical source(several tens of μm for a 20-nm bandwidth).

A realistic practical level is generally accepted to be around 1 cm which implies the use of optical bandwidths of $\sim$0.1 nm, or less. It is not easy to obtain such a laser linewidth directly from an oscillator, however it is readily achieved using narrowband ASE sources. For example, using FBG technology it is possible to fabricate filters of almost arbitrary spectral shape (and width) with which to spectrally slice the output from conventional broad-band sources, providing a powerful and flexible means of generating light of well-controlled (and defined) coherence properties. It should be apparent that in contrast to the use of broad-band ASE sources, narrowband ASE also has the advantage of offering increased scope for sensor multiplexing through the use of WDM technology when used with appropriate narrowband FBG-based sensing interferometers. However, there is a major issue concerned with the use of narrowband ASE sources that needs to be addressed—that of source noise.

It is known that fiber ASE sources exhibit thermal source-like noise properties [9], characterized in terms of excess photon noise [10], [11]. As we shall show below, ASE sources exhibit significant intensity noise relative to conventional lasers and this noise power increases in proportion to the reciprocal bandwidth of the source. Indeed, in most optical systems employing ASE sources, the system performance is ultimately limited by the optical source noise.

Manuscript received May 24, 1999; revised July 13, 1999. This work was funded in part by the U.K. EPSRC Grant GR/L87057, Sensor Dynamics Ltd., U.K., and Geosensor Corporation, USA.

The authors are with the Optoelectronics Research Center, University of Southampton, Southampton SO17 1BJ, U.K. (e-mail: hsk@orc.soton.ac.uk).

Publisher Item Identifier S 0733-8724(99)08804-0.

Clearly then, it is important to establish the impact of source noise on the use of narrowband ASE for the interrogation of interferometers. It is well established that the statistical properties of thermal light can be explained on the basis of a Gaussian random process model [12]. However, an estimate of the true impact of the source noise on a given systems performance is complicated by the filtering effect in multiple-path optical systems, such as interferometers [13], [14], which can cause redistribution of the optical noise power in the spectral domain. Note that this is also true of components such as polarization modulators and frequency shifters frequently incorporated within such systems for functions such as polarization control, and heterodyne signal processing. Consequently, in order to appreciate the full impact of the higher levels of source noise, and to assess the true potential of the approach, we need to consider in detail the full interferometer system. In earlier works [14], [15], a suitable mathematical formulation applicable to the use of a generalized low coherence source was developed and applied to a few simple systems. In this paper, we have focused our study on the use of an erbium fiber-based, narrowband ASE source for the interrogation of Mach–Zehnder interferometers, which are one of the leading candidates for coherence-multiplexed systems. We generalize the earlier theoretical approach to include the effects of birefringence in the optical paths and to cover the inclusion of a frequency shifter (as required for heterodyne-based demodulation schemes) and then compare the results of our detailed noise analysis with our experimental data. Our results show that minimum phase sensitivities of a few tens of μrad/$\sqrt{\text{Hz}}$ can be achieved for practical values of length mismatch by optimization of the source linewidth, heterodyne frequency, and interferometer birefringence.

The paper structure is as follows. In Section II, we first outline the basic theory used to describe the noise properties of thermal source noise. We then describe the specific narrowband ASE source we have developed and used within our experiments and present results of noise measurements that show that its noise properties truly correspond to those of an idealized thermal source. In Section III, the noise properties of a dual Mach–Zehnder interferometer are treated theoretically, and the predictions compared with experiment. In Section IV, we extend the results of section to include the effects of a frequency shifter within the system, once again comparing the theoretical results with experimental data. The conclusions of our studies are summarized in Section V.

II. Noise Properties of Narrowband ASE Sources

A. Theory

In almost all optical systems, the physical quantity ultimately measured, and from which the useful information is derived, is the current of a photodetector. Optical source noise measurements are also most usually and conveniently derived from current measurements. It is well known that the noise spectrum can be obtained from the Fourier transform of the covariance function of the current Cov_i which is defined as [14], [16]

$$\mathrm{Cov}_i(\tau) = \langle (i(t)i(t+\tau)\rangle - \langle i(t)\rangle^2 \tag{1}$$

where $i(t)$ is the detector current at time t, τ is the time delay, and $\langle\cdots\rangle$ denotes the time-averaged value. The (electrical) noise spectrum $S(f)$ at a frequency f can be written as

$$S(f) = R\int_{-\infty}^{\infty} \mathrm{Cov}_i(\tau)e^{2\pi i f\tau}\,d\tau \tag{2}$$

where R is the output load resistance of the detector. The current $i(t)$ in the above equations can be substituted by the optical intensity at the detector $I(t)$ when we consider only the noise component due to the optical source itself, and (1) can thus be written as

$$\begin{aligned}\mathrm{Cov}_i(\tau) &= \alpha^2\mathrm{Cov}_I(\tau)\\ &= \alpha^2\left(\langle (I(t)I(t+\tau)\rangle - \langle I(t)\rangle^2\right)\end{aligned} \tag{3}$$

where α is a conversion factor from the optical intensity to electrical current.

For a polarized thermal source $\mathrm{Cov}_I(\tau)$ can also be expressed as

$$\mathrm{Cov}_I(\tau) = |\Gamma(\tau)|^2 \equiv |\langle E^*(t)E(t+\tau)\rangle|^2 \tag{4}$$

where $E(t)$ is the electric field of the optical source and $\Gamma(\tau)$ is the correlation function of the electric field [17]. If the optical spectrum of the source is

$$I(\nu) = I_0\Psi(\nu-\nu_0) \tag{5}$$

$\Gamma(\tau)$ can be written as

$$\Gamma(\tau) = I_0e^{-2\pi i\nu_0\tau}\int_{-\infty}^{\infty}\Psi(x)e^{-2\pi ix\tau}\,dx \tag{6}$$

and by the Wiener–Khintchine theorem, the (*electrical*) noise power spectrum $S(f)$ can be written as

$$S(f) = \alpha^2I_0^2R\int_{-\infty}^{\infty}\Psi\left(x-\frac{f}{2}\right)\Psi\left(x+\frac{f}{2}\right)dx \tag{7}$$

where I_0 is the intensity of the optical source, ν is the optical frequency, ν_0 is the center frequency of the source, and $\Psi(x)$ is the normalized envelop function of the optical spectrum with a center frequency of zero. From (7), we can understand that the noise power at the frequency f is the summation of all pairs of spectral components whose frequency difference is f.

If for the moment we assume a Gaussian spectral profile $I(\nu)$, i.e.,

$$I(\nu) = \frac{I_0}{\Delta\nu_0}\sqrt{\frac{4\log_e 2}{\pi}}\exp\left[-4\log_e 2\,\frac{(\nu-\nu_0)^2}{\Delta\nu_0^2}\right] \tag{8}$$

where $\Delta\nu_0$ is the full-width-half-maximum of the optical spectrum, then one can use (7) to obtain the well established result that

$$S(f) = \frac{\alpha^2I_0^2R}{\Delta\nu_0}\sqrt{\frac{2\log_e 2}{\pi}}\exp\left[-2\log_e 2\,\frac{f^2}{\Delta\nu_0^2}\right]. \tag{9}$$

The above equation shows the following important noise characteristics of thermal light. First, that the noise power

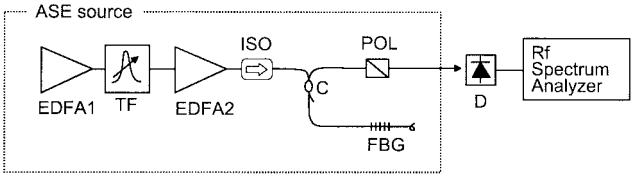

Fig. 1. Experimental setup for the measurement of the optical source noise spectrum. EDFA's: erbium-doped fiber amplifiers, TF: tunable filter, POL: polarizer, C: 50 : 50 coupler, FBG: fiber Bragg grating, D: detector, ISO: optical isolator.

TABLE I
CHARACTERISTICS OF FIBER BRAGG GRATINGS

ID	Centerwavelength (nm)	FWHM (pm)	FWHM (GHz)
FBG1	1559.6	18	2.2
FBG2	1545.8	45	5.6
FBG3	1529.5	60	7.7
FBG4	1529.3	81	10.4
FBG5	1529.3	115	14.7

scales with the square of the optical intensity and, second and most significantly from the perspective of this study, the inverse linewidth. The price we are to pay for the advantage of multiplexing capability and length mismatch tolerance is increased optical noise.

B. Noise Performance of Experimental Narrowband ASE Source

The experimental setup used to characterize the noise properties of narrowband ASE is shown in Fig. 1. The source itself comprised two erbium doped erbium fiber amplifiers and two spectral filters. The first stage erbium-doped fiber amplifier (EDFA) was used as a broad-band optical source, the output from this was filtered with a tunable filter of 1.3-nm bandwidth and then amplified in the second EDFA to increase the spectral power density around the center-wavelength of the tunable filter. The output from the second amplifier was then spectrally filtered using a narrowband FBG whose reflectivity spectrum ultimately defined the output spectral profile of the source. The tunable filter's central wavelength was obviously tuned to match the peak reflectivity wavelength of the FBG. The filtered output was coupled off of the grating using a 50 : 50 coupler and polarized using a fiber polarizer. We had five narrowband FBG's each of different spectral linewidths (in the range ≈2–15 GHz, see Table I) and could therefore easily vary the spectral bandwidth and line shape of the source simply by changing the output FBG.

The source output noise was first characterized using an RF spectrum analyzer and a fiber coupled, low-noise, InGaAs detector incorporating a transimpedance amplifier of 200 MHz bandwidth with an optical power to current conversion factor α of 360 A/W using a load resistance of 50 Ω.

Initially, we measured the spectral noise power at three different frequencies (1, 10, and 100 MHz) as a function

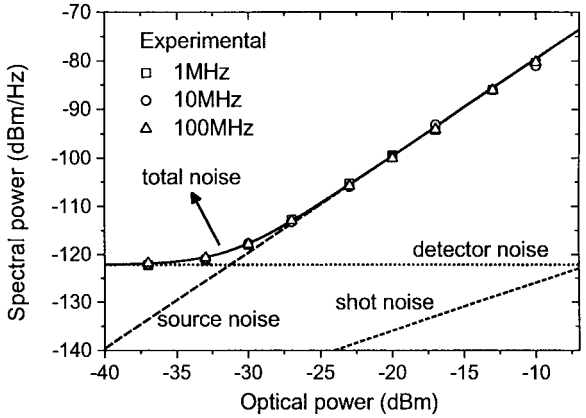

Fig. 2. Spectral noise power versus optical power. The three symbols are the measured noise at the frequency of 1 MHz (square), 10 MHz (circle), and 100 MHz (triangle). The lines (except the detector noise) are obtained from theory.

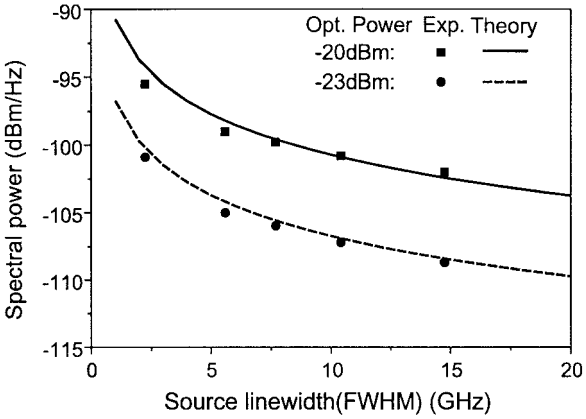

Fig. 3. Spectral noise power versus source linewidth. Measurement frequency was 10 MHz.

of received optical power for the grating FBG3, and also calculated the noise power using the measured reflectivity profile. The experimental results (total noise power spectral density) are summarized in Fig 2. Superposed on the graph are plots showing the detector noise (experimental), and theoretical plots showing the calculated ASE source noise, shot noise, and total noise. The experimental results are in good agreement with theory confirming the intensity-squared dependence of the noise power. At frequencies substantially less than the optical linewidth of the source, the optical power at which the ASE noise becomes larger than shot noise is −56 dBm. The relative intensity noise (RIN) of this source was −97.7 dB/Hz. Note that the spectral noise power density is flat over the detector bandwidth due to the relatively broad linewidth of the source compared to the detection bandwidth.

Fig. 3 shows the measured and the calculated spectral noise power at 10 MHz as a function of source linewidth for optical powers of −20 and −23 dBm. The actual reflectivity profile of FBG3 was used in the theoretical noise calculations. The results confirm the predicted noise dependency on inverse linewidth.

As is apparent from (7), the detailed shape of the ASE source noise is directly related to the optical lineshape. To

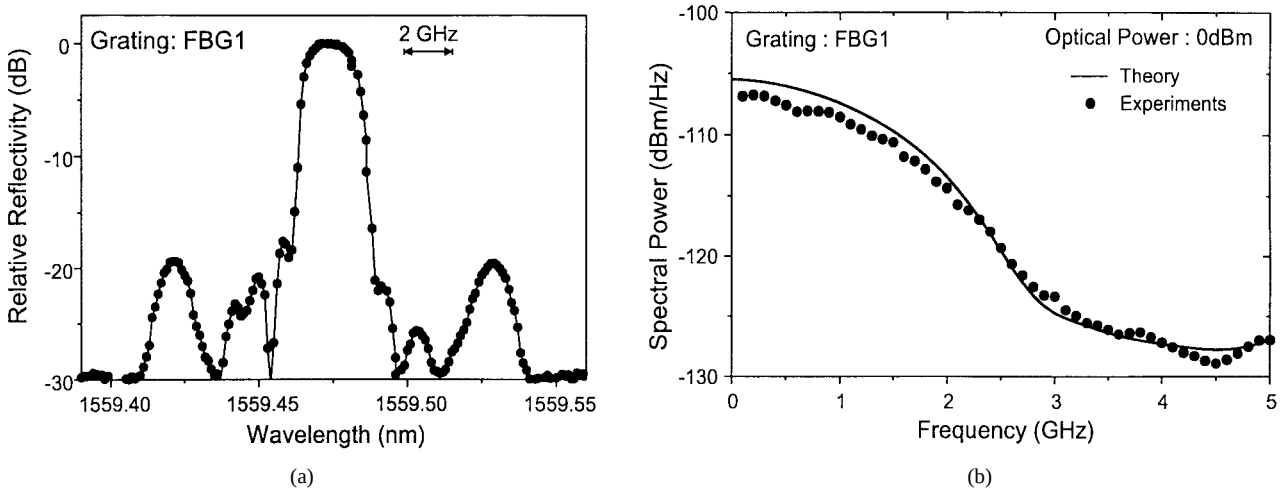

(a) (b)

Fig. 4. Reflectivity profile of FBG1 and noise spectrum: (a) relative reflectivity of FBG1 and (b) noise power spectrum.

confirm this to be the case, we measured the noise spectrum of the ASE source with a fast (6 GHz bandwidth) detector. The ASE source optical lineshape was defined by FBG1 in this instance. Since the source noise decreases at high frequencies, a further EDFA was included after the polarizer to boost the source noise level above the detector noise floor in the high-frequency regime. The ASE input power to the additional EDFA was −13 dBm, and the output power was set to be 0 dBm. The reflectivity profile of the grating FBG1 is shown in Fig. 4(a), and the measured and theoretical noise spectrum, calculated using the FBG1 reflectivity profile in (7), are shown in Fig. 4(b), the agreement is seen to be good.

From the above results, it is clear that our narrowband ASE source behaves as expected and that its noise properties are well described using a Gaussian random process model. This model can thus be used with confidence to predict the noise properties of a variety of interferometer interrogation systems employing such sources.

III. Dual Mach–Zehnder Interferometer

As previously discussed, estimating the noise level for an interferometer is not straightforward. The filtering effect due to the multiple optical paths significantly modifies the noise distribution and leads to periodic structure in the frequency domain. Note also, that this noise distribution is a function of the birefringence within the system. We demonstrate the above two features in the following section, in which we evaluate, both analytically and experimentally, the noise properties of dual Mach–Zehnder interferometer systems. The precise system we are considering is shown in Fig. 5(a). In our calculations we assume for simplicity that the coupling ratio of the couplers is 50 : 50, and that the relative time delays, T_1 and T_2, are much longer than the coherence time of the optical source.

In order to understand the effects of birefringence within the interferometer, we considered the two extreme cases, shown in Fig. 5(b) and (c). In the first case, Fig. 5(b), the polarization of the light passing through the two paths of each Mach–Zehnder interferometer is the same (*polarization preserving (PP) case*).

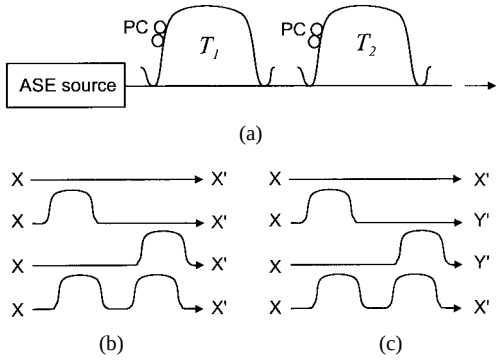

(a) (b) (c)

Fig. 5. Dual Mach–Zehnder interferometer: (a) schematics, (b) PP case, and (c) PF case.

In the second case, the polarization state of the light in one arm of each interferometer is changed to be orthogonal to the light in the other arm (*polarization flipping (PF) case*). Both cases result in maximum visibility for the interferometer.

A. Theory for the "Polarization Preserving Case"

The output electric field E_{out}, and the coherence function of the output intensity $\Gamma_{\text{out}}(\tau)$ are

$$E_{\text{out}}(t) = \frac{1}{2^2}\left[E(t) + E(t-T_1) + E(t-T_2) + E(t-T_1-T_2)\right] \tag{10}$$

$$\begin{aligned}\Gamma_{\text{out}}(\tau) &= \langle E^*_{\text{out}}(t) E_{\text{out}}(t+\tau)\rangle \\ &= \frac{1}{2^4}\{4\Gamma(\tau) + 2\Gamma(\tau+T_1) \\ &\quad + 2\Gamma(\tau-T_1) + 2\Gamma(\tau+T_2) + 2\Gamma(\tau-T_2) \\ &\quad + \Gamma(\tau+T_1+T_2) + \Gamma(\tau-T_1-T_2) \\ &\quad + \Gamma(\tau+\Delta T) + \Gamma(\tau-\Delta T)\}\end{aligned} \tag{11}$$

where $\Delta T = T_2 - T_1$. Note, that for convenience, the relative $\pi/2$ phase-shift which occurs between the two arms of the coupler is not included in (10) since it is irrelevant to the overall results of the analysis. The covariance function of the output $\text{Cov}_I(\tau)$ can be written as

$$\text{Cov}_I(\tau) = |\Gamma_{\text{out}}(\tau)|^2 \tag{12}$$

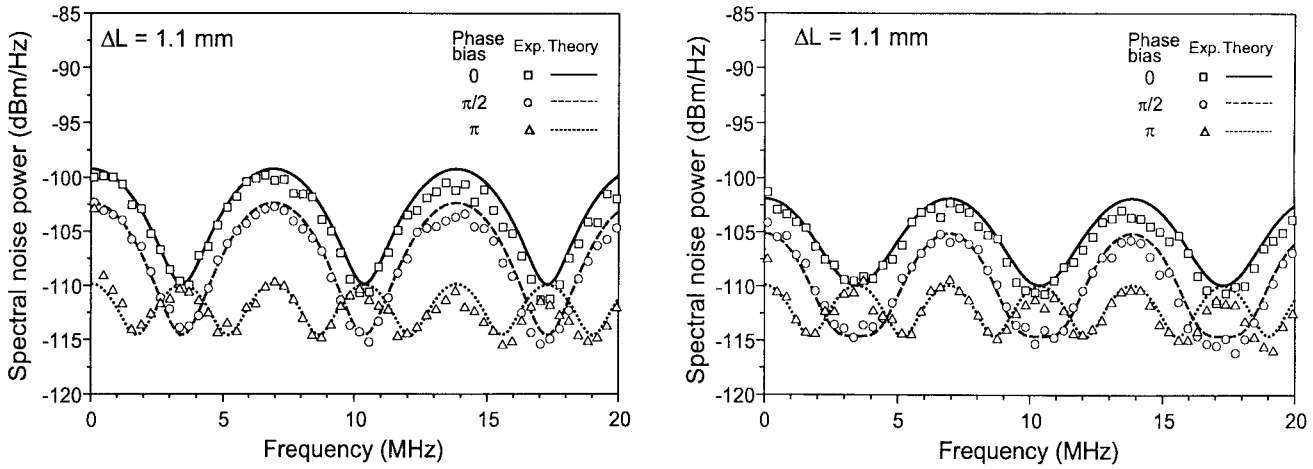

(a) (b)

Fig. 6. Noise spectra of the dual Mach–Zehnder interferometer: (a) PP case and (b) PF case.

and has 81 terms in this case. Each term is of the form $\Gamma^*(\tau+T_i)\Gamma(\tau+T_j)$, and provides a contribution to the total noise spectrum $S_{ij}(f)$ of

$$S_{ij}(f) = \frac{\alpha^2 R}{2^8}\int_{-\infty}^{\infty}\Gamma^*(\tau+T_i)\Gamma(\tau+T_j)e^{2\pi i f\tau}\,d\tau \tag{13}$$

$$= \frac{\alpha^2 I_0^2 R}{2^8}e^{-2\pi i\nu_0(T_j-T_i)}e^{-\pi i f(T_j+T_i)} \cdot\left[\int_{-\infty}^{\infty}\Psi\left(x-\frac{f}{2}\right)\Psi\left(x+\frac{f}{2}\right)e^{-2\pi i x(T_j-T_i)}\,dx\right]. \tag{14}$$

The term in square brackets in the previous equation can be ignored when $|T_i-T_j|$ is much larger than the coherence time of the source. Therefore, $\mathrm{Cov}_I(\tau)$ can be written as

$$\begin{aligned}\mathrm{Cov}_I(\tau) = \frac{1}{2^8}\{&16|\Gamma(\tau)|^2+4|\Gamma(\tau+T_1)|^2+4|\Gamma(\tau-T_1)|^2\\ &+4|\Gamma(\tau+T_2)|^2+4|\Gamma(\tau-T_2)|^2\\ &+|\Gamma(\tau+(T_1+T_2))|^2+|\Gamma(\tau-(T_1+T_2))|^2\\ &+|\Gamma(\tau+\Delta T)|^2+|\Gamma(\tau-\Delta T)|^2\\ &+[4\Gamma^*(\tau)(\Gamma(\tau+\Delta T)+\Gamma(\tau-\Delta T))+\text{c.c.}]\\ &+[4\Gamma^*(\tau+T_1)\Gamma(\tau+T_2)+\text{c.c.}]\\ &+[4\Gamma^*(\tau-T_1)\Gamma(\tau-T_2)+\text{c.c.}]\\ &+[\Gamma^*(\tau+\Delta T)\Gamma(\tau-\Delta T)+\text{c.c.}]\}\end{aligned} \tag{15}$$

when the terms which give insignificant contribution to the noise spectrum are ignored. Here c.c. denotes complex conjugate.

To simplify the calculation, we assume from now on that the optical spectrum of the source is symmetric about it's center frequency, i.e., $\Psi(-x)=\Psi(x)$, a condition satisfied to a good approximation in our current experiments. With this assumption the noise spectrum can be written as

$$\begin{aligned}S(f) = \frac{\alpha^2 I_0^2 R}{2^8}&\{4F(f,0)[(2+\cos 2\pi f T_1)(2+\cos 2\pi f T_2)]\\ &+32F(f,\Delta T)\cos\pi f T_1\cos\pi f T_2\cos 2\pi\nu_0\Delta T\\ &+2F(f,2\Delta T)\cos 4\pi\nu_0\Delta T\}\end{aligned} \tag{16}$$

where $F(f,T)$ is

$$F(f,T)=\int_{-\infty}^{\infty}\Psi\left(x-\frac{f}{2}\right)\Psi\left(x+\frac{f}{2}\right)e^{-2\pi i x T}\,dx. \tag{17}$$

From (16) two things are immediately apparent. First, the noise spectrum exhibits periodicity in the frequency domain (see Fig. 6), the period of which is defined by the time delays T_1 and T_2. This effect is well known and is referred to as the "filtering effect" of the interferometer [13]. Second, the noise spectrum is highly dependent on the relative phase bias $\Delta\phi(=2\pi\nu_0\Delta T)$. These points will be discussed again in relation to the experimental results presented below.

B. Theory for "Polarization Flipping Case"

In this case we need to consider separately the noise interference effects within the two polarization eigenstates of the system. In this case the output electric field is given by

$$\begin{aligned}E_{\text{out}}(t) &= \mathbf{e}_{x'}E_{x'}(t)+\mathbf{e}_{y'}E_{y'}(t)\\ &= \frac{1}{2^2}\{\mathbf{e}_{x'}[E(t)+E(t-T_1-T_2)]\\ &\quad+\mathbf{e}_{y'}[E(t-T_1)+E(t-T_2)]\}\end{aligned} \tag{18}$$

and $\mathrm{Cov}_I(\tau)$ is given as

$$\begin{aligned}\mathrm{Cov}_I(\tau) = \frac{1}{2^8}\{&8|\Gamma(\tau)|^2+2|\Gamma(\tau+T_1)|^2+2|\Gamma(\tau-T_1)|^2\\ &+2|\Gamma(\tau+T_2)|^2+2|\Gamma(\tau-T_2)|^2\\ &+|\Gamma(\tau+(T_1+T_2))|^2+|\Gamma(\tau-(T_1+T_2))|^2\\ &+|\Gamma(\tau+\Delta T)|^2+|\Gamma(\tau-\Delta T)|^2\\ &+[2\Gamma^*(\tau)(\Gamma(\tau+\Delta T)+\Gamma(\tau-\Delta T))+\text{c.c.}]\\ &+[2\Gamma^*(\tau+T_1)\Gamma(\tau+T_2)+\text{c.c.}]\\ &+[2\Gamma^*(\tau-T_1)\Gamma(\tau-T_2)+\text{c.c.}]\\ &+[\Gamma^*(\tau+\Delta T)\Gamma(\tau-\Delta T)+\text{c.c.}]\}.\end{aligned} \tag{19}$$

After more patient analysis, it can be shown that in this case the noise spectrum can be written as

$$S(f) = \frac{\alpha^2 I_0^2 R}{2^8}\{4F(f,0)[1+(1+\cos 2\pi f T_1)\cdot(1+\cos 2\pi f T_2)] + 16F(f,\Delta T)\cos \pi f T_1 \cdot \cos \pi f T_2 \cos 2\pi \nu_0 \Delta T + 2F(f,2\Delta T)\cdot \cos 4\pi \nu_0 \Delta T\}. \quad (20)$$

Once again, a periodically modulated noise spectrum is obtained, however, the detailed form of the noise is actually significantly different relative to the PP case. The main conclusion of the analysis is that the PF case has reduced noise levels relative to the PP case in an appropriately designed interferometer system, as demonstrated in the following section (see Fig. 6).

C. Experiments and Discussions

In order to validate the above analysis we constructed a dual MZ system and examined its noise properties when interrogated with the narrowband ASE source described previously (incorporating FBG3). The delay length in each of the interferometers was ∼29.6 m. The coupling ratios of all couplers was 50 : 50, and polarization controllers were placed in each interferometer to enable us to set the polarization states throughout the system for the PP and PF cases previously described. A piezoelectric fiber stretcher was included within the first interferometer to allow us to adjust the relative phase of the two interferometers. We measured the noise spectrum in the frequency range of 0–20 MHz for the PP and PF cases, for two values of length mismatch between the interferometers (1.1 and 9.3 mm), and for three values of phase bias. The length mismatches were measured using a broad-band optical source and an optical spectrum analyzer. Since the output power was a function of the phase bias the output power at the phase bias of $\pi/2$ was set to be -23 dBm for all measurements.

The polarization controllers were set as follows for the PP and PF cases. First, we introduced a large bend loss in one of the arms of the second interferometer, and set the polarization controller in the first interferometer such that the spectral noise power was either maximized, (or minimized). This allowed us to set the output polarization states of the light passing through the two different paths in the first interferometer to be either mutually parallel, (or orthogonal) [14]. Next, we removed the bend loss in the second interferometer, and set the polarization controller within this interferometer to maximize the signal visibility, resulting in either the PP, (or PF) configuration.

Fig. 6 shows the noise spectra for the three different phase bias points, for the length mismatch of 1.1 mm, and for the different polarization cases. The noise redistribution properties of the interferometer are immediately apparent, recall from Fig. 2, that the source noise itself is a uniform -105.6 dBm/Hz over this frequency range for a fixed optical power of -23 dBm. The agreement between the experimental and theoretical noise spectra is good. For the phase bias of $\pi/2$ in Fig. 6 the noise spectrum has a period of 6.92 MHz, which corresponds to the inverse of the elapsed time for light to pass through the path imbalance of the individual interferometers. The noise power is highest (-99 dBm/Hz) at 0 relative phase bias at the spectral maxima (e.g., at 7.62 MHz), and falls to its smallest value of -115 dBm/Hz at the noise minima (e.g., at 3.46 MHz) for a bias of $\pi/2$. The maximum noise level difference (maxima to minima) at fixed phase bias is about 12 dB for the $\pi/2$ phase bias.

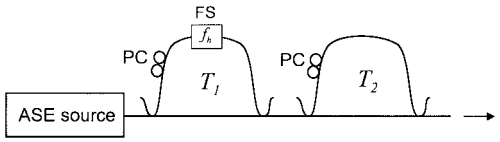

Fig. 7. Dual Mach–Zehnder interferometer using a frequency shifter.

For the PF case the general features of the noise redistribution were much the same, although there are slight differences in the detailed spectral shape. The most important difference is that the maximum noise power is about 2.5 dB lower in this instance (0 phase bias). The experimental results for the length mismatch of 9.3 mm showed the same features, although the dependence of the phase bias became weaker due to the lower signal visibility (∼0.3), compared to the former case (∼0.48).

From these results, it is clear that a higher overall sensitivity might be achieved for such an interferometer system by using the periodicity in the noise spectrum, simply by moving the signal frequency (typically in the low-frequency regime), to a spectral region with a minima in the noise distribution. This can be readily achieved by incorporating a frequency shifter into the system, and operating in a heterodyne fashion, as demonstrated in the next section.

IV. Dual Mach–Zehnder Interferometer Incorporating a Frequency Shifter

The heterodyne technique is frequently used in interferometer systems to avoid the high noise levels at low frequency and thereby to achieve high sensitivity. In our system this is most readily implemented by including a frequency shifter in one of the arms of the first (reference) Mach–Zehnder interferometer (see Fig. 7). When a modulator is employed in the system, the modulation changes not only the signal distribution in the spectral domain, but also the noise distribution as we show below, both theoretically and experimentally, for both the PP and PF configurations previously described.

A. Polarization Preserving Case

The output intensity $I_{\text{out}}(t)$ is in this instance given by

$$I(t) = \frac{1}{2^4}\left|E(t) + E(t-T_1)e^{2\pi i f_h t} + E(t-T_2) + E(t-T_1-T_1)e^{2\pi i f_h t}\right|^2 \quad (21)$$

and, after some effort, the covariance function can be expressed as

$$\begin{aligned}\mathrm{Cov}_I(\tau) = \frac{1}{2^8}\{&[2|\Gamma(\tau+T_1)|^2 + 2|\Gamma(\tau-T_1)|^2 \\ &+ 2|\Gamma(\tau+T_2)|^2 + 2|\Gamma(\tau-T_2)|^2 \\ &+ |\Gamma(\tau+T_1+T_2)|^2 + |\Gamma(\tau-T_1-T_2)|^2 \\ &+ |\Gamma(\tau+\Delta T)|^2 + |\Gamma(\tau-\Delta T)|^2 \\ &+ 8|\Gamma(\tau)|^2 + 2|\Gamma(\tau+T_1)|^2 + 2|\Gamma(\tau-T_1)|^2] \\ &+ [(4|\Gamma(\tau)|^2 + |\Gamma(\tau+T_2)|^2 + |\Gamma(\tau-T_2)|^2) \\ &\quad \cdot (e^{2\pi i f_h \tau} + e^{-2\pi i f_h \tau})] \\ &+ [|\Gamma(\Delta T)|^2 (e^{2\pi i f_h \tau} + e^{-2\pi i f_h \tau})]\}. \end{aligned} \tag{22}$$

Note that (12) is not applicable in this case due to the frequency shift term. In order to derive (22), we used the original definition of $\mathrm{Cov}_I(\tau)$ shown in (3) and calculated $\langle I(t)I(t+\tau)\rangle$ and $\langle I(t)\rangle^2$ separately using the following relation:

$$\left\langle E^*(t_1)E(t_2)E^*(t_3)E(t_4)e^{2\pi i f_h t}\right\rangle = 0. \tag{23}$$

The noise spectrum can then be shown to be given by the following expression:

$$\begin{aligned}S(f) = \frac{\alpha^2 I_0^2 R}{2^8}\{&4F(f,0)[(1+\cos 2\pi f T_1)(2+\cos 2\pi f T_2)] \\ &+ F(f-f_h,0)[4+2\cos 2\pi(f-f_h)T_2] \\ &+ F(f+f_h,0)[4+2\cos 2\pi(f+f_h)T_2] \\ &+ |\Gamma(\Delta T)|^2[\delta(f-f_h)+\delta(f+f_h)]\} \end{aligned} \tag{24}$$

where $\delta(x)$ is the delta function.

B. Polarization Flipping Case

In this instance the intensity $I_{\mathrm{out}}(t)$ is

$$\begin{aligned}I_{\mathrm{out}}(t) = \frac{1}{2^4}\Big[&\left|E(t)+E(t-T_1-T_2)e^{2\pi i f_h \tau}\right|^2 \\ &+ \left|E(t-T_2)+E(t-T_1)e^{2\pi i f_h \tau}\right|^2\Big]. \end{aligned} \tag{25}$$

The covariance function $\mathrm{Cov}_I(\tau)$ can be expressed as

$$\begin{aligned}\mathrm{Cov}_I(\tau) = \frac{1}{2^8}\{&4|\Gamma(\tau)|^2 + 2|\Gamma(\tau+T_1)|^2 + 2|\Gamma(\tau-T_1)|^2 \\ &+ 2|\Gamma(\tau+T_2)|^2 + 2|\Gamma(\tau-T_2)|^2 \\ &+ |\Gamma(\tau+T_1+T_2)|^2 + |\Gamma(\tau-T_1-T_2)|^2 \\ &+ |\Gamma(\tau+\Delta T)|^2 + |\Gamma(\tau-\Delta T)|^2 \\ &+ [2|\Gamma(\tau)|^2 (e^{2\pi f_h i\tau} + e^{-2\pi i f_h \tau})] \\ &+ [|\Gamma(\Delta T)|^2 (e^{2\pi i f_h \tau} + e^{-2\pi i f_h \tau})]\}. \end{aligned} \tag{26}$$

The noise spectrum is given by

$$\begin{aligned}S(f) = \frac{\alpha^2 I_0^2 R}{2^8}\{&4F(f,0)[(1+\cos 2\pi f T_1)(1+\cos 2\pi f T_2)] \\ &+ 2F(f-f_h,0)\cos 2\pi(f-f_h)T_2 \\ &+ 2F(f+f_h,0)\cos 2\pi(f+f_h)T_2 \\ &+ |\Gamma(\Delta T)|^2(\delta(f-f_h)+\delta(f+f_h))\}. \end{aligned} \tag{27}$$

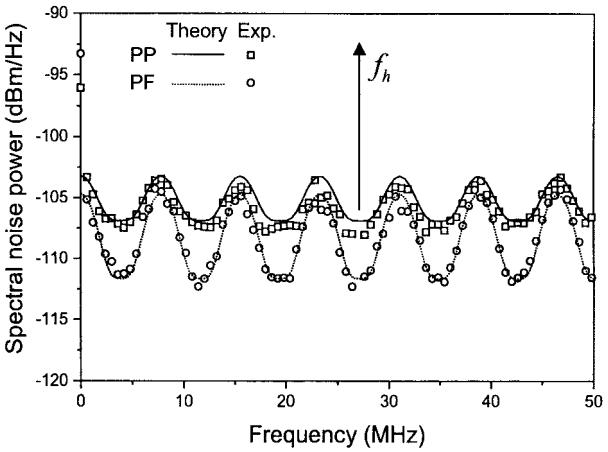

Fig. 8. Noise spectra of the dual MZ interferometer using heterodyne method.

The terms containing $F(f \pm f_h)$ in (24) and (27) imply noise redistribution due to the frequency shift f_h and the terms containing $\delta(f \pm f_h)$ correspond to the carrier signal in the heterodyne method. Once again the noise spectrum is found to exhibit periodic structure, although in this instance the issue of relative phase bias between the two interferometers ceases to be of any significance. Plots showing the noise redistribution properties for both the PP and PF for a particular implementation of this system are shown in Fig. 8 and compared with experiment in the following section.

Note that when a small signal $\phi_s \sin(2\pi f_s t)$ is applied to the one of the interferometers, the signal power spectrum $S_{sig}(f)$ can be written as

$$\begin{aligned}S_{sig}(f) = \frac{\alpha^2 I_0^2 R}{2^4}\Big\{&4\delta(f) + V^2[\delta(f-f_h)+\delta(f+f_h)] \\ &+ V^2\frac{(\phi_s)^2}{2^2}[\delta(f-(f_h-f_s))+\delta(f-(f_h+f_s)) \\ &+ \delta(f+(f_h-f_s))+\delta(f+(f_h+f_s))]\Big\} \end{aligned} \tag{28}$$

where V is twice the signal visibility and is given by

$$V = \left|\int_{-\infty}^{\infty} \Psi(x) e^{-2\pi i(T_2-T_1)}\, dx\right|. \tag{29}$$

The minimum theoretical detectable phase can thus readily be obtained by equating the signal spectrum in (28) to the noise spectral density at the signal frequency $f_h \pm f_s$.

C. Experiments and Discussion

We built the dual Mach–Zehnder interferometer incorporating a frequency shifter shown in Fig. 7 to validate the above theory. The delay length of each Mach–Zehnder interferometer was 26.52 m, a length chosen to minimize the noise around the heterodyne frequency of 27.12 MHz, as defined by the frequency shifter. A PZT phase modulator was inserted in one of the arms of the second interferometer to allow us to apply a well defined level of phase modulation. Polarization controllers were included in the system to allow us to set the polarizations within the system for either PP or PF implementations. We performed experiments for length

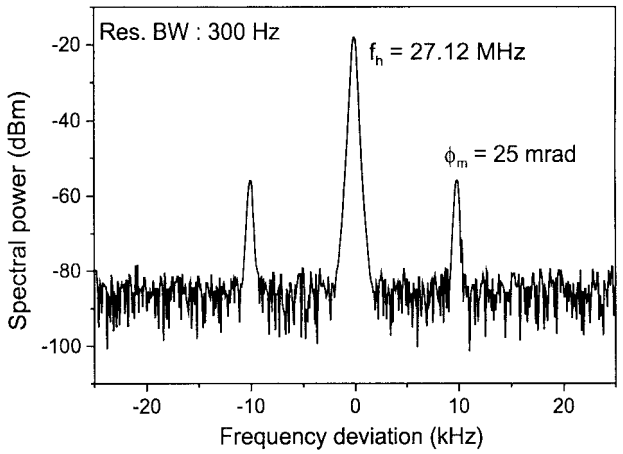

Fig. 9. Signal and noise corresponding to system parameters described within the text.

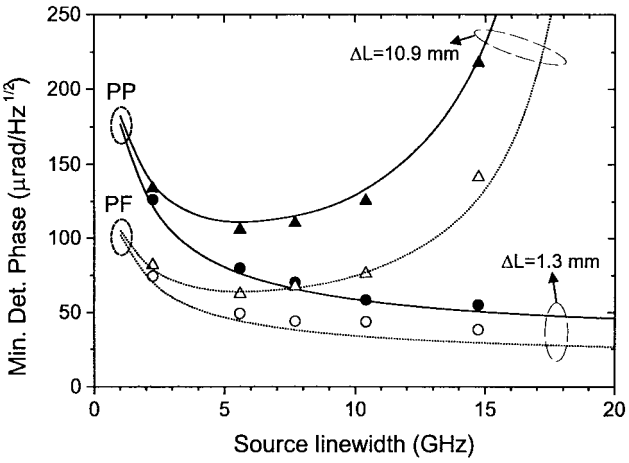

Fig. 10. Minimum detectable phase versus source linewidth.

mismatches of 1.3 and 10.9 mm. The length mismatches were estimated from the periods of the measured noise spectra of the individual interferometers to a resolution of ± 0.6 mm. The average optical power was set to -23 dBm throughout.

Fig. 8 shows the noise spectra for the source linewidth of 7.7 GHz obtained from both theory and experiments for the different polarization settings, and for a length mismatch of 1.3 mm. The noise level of the PF case is seen to be smaller than that of the PP case over the full detection bandwidth, falling to -112 dBm at the spectral minima. In both cases the signal power is the same for a fixed level of phase modulation (via the PZT). The noise level is thus substantially lower ($\sim$5 dB) for the PF case. Similar patterns and levels of noise redistribution were obtained for other values of source linewidth and length mismatch. The minimum detectable phase was measured by applying a known level of phase modulation to the PZT and observing the heterodyne signal and noise floor on an RF spectrum analyzer. Fig. 9 shows the spectrum with the resolution bandwidth of 300 Hz when a phase modulation of 25 mradian was applied for the PF case. The minimum detectable phase was 44 μrad/$\sqrt{\text{Hz}}$ in this instance.

Measurements were made as a function of source linewidth for the two length mismatches of 1.3 and 10.9 mm, and for both PP and PF polarization settings. The results are shown in Fig. 10, superposed are theoretical curves derived using (24) and (27). Good agreement between experiment and theory is obtained. Note that all parameters used in the theoretical curves are measured—there are no free/fit parameters in the theory. From Fig. 10 it is seen that a minimum detectable phase of 62 μrad/$\sqrt{\text{Hz}}$ is obtained for the practical length mismatch of 10.9 mm. The minimum value is obtained for a linewidth of $\sim$5 GHz. At narrower source linewidths the increased source noise reduces the sensitivity, whilst at broader linewidths the rapidly reducing signal visibility limits performance. For smaller, (but impractical), length mismatches significantly lower minimum detectable phases can be achieved. For example, values as low as 25 μrad/$\sqrt{\text{Hz}}$ for a source linewidth of 20 GHz are predicted. These results validate our theory and provide important information as to how to design an optimized system for any level of practical limitation on length mismatch, source linewidth, sensor length, etc.

V. Conclusion

In conclusion, we have investigated both experimentally and theoretically the noise characteristics and sensitivity limits of dual fiber Mach–Zehnder interferometers interrogated using narrowband fiber ASE sources. We have shown that the system performance is limited by the excess photon noise of the source and that the detailed system noise spectrum is dependent on the filtering effect and birefringence in the optical paths of the interferometer. By employing a heterodyne technique and utilizing these noise redistribution effects, we have shown that it is possible to reduce the noise level in the signal frequency region and have achieved a minimum detectable phase of 62 μrad/$\sqrt{\text{Hz}}$, for a practical path length mismatch of $\sim$1 cm. We consider the approach we have demonstrated to be highly practical, providing good phase resolution while remaining consistent with interferometer manufacturing tolerances and requiring relatively simple demodulation methods.

Acknowledgment

The authors wish to thank Dr. M. Varnham of Sensor Dynamics Ltd. (U.K.) for useful discussions and M. Ibsen for providing the fiber gratings used in these experiments. H. S. Kim would like to thank Dr. R. Feced for valuable discussions.

References

[1] J.-H. Han, J.-W. Ko, J.-S. Lee, and S.-Y. Shin, "0.1-nm narrow bandwidth transmission of a 2.5-Gb/s spectrum-sliced incoherent light channel using an all-optical bandwidth expansion technique at the receiver," *IEEE Photon. Technol. Lett.*, vol. 10, pp. 1501–1503, Oct. 1998.

[2] J. L. Wagener, M. J. F. Digonnet, and H. J. Shaw, "A high-stability fiber amplifier source for the fiber optic gyroscope," *J. Lightwave Technol.*, vol. 15, pp. 1689–1694, Sept. 1997.

[3] A. D. Kersey, M. A. Davis, H. J. Patrick, M. L. LeBlanc, K. P. Koo, C. G. Askins, M. A. Putnam, and E. J. Friebele, "Fiber grating sensors," *J. Lightwave Technol.*, vol. 15, pp. 1442–1463, Aug. 1997.

[4] J. L. Brooks, R. H. Wentworth, R. C. Youngquist, M. Tur, B. Y. Kim, and H. J. Shaw, "Coherence multiplexing of fiber-optic interferometric sensors," *J. Lightwave Technol.*, vol. LT-3, pp. 1062–1071, Oct. 1985.

[5] K. Iiyama and K. Hayashi, "Frequency domain detection of coherence multiplexed sensor signals by using an optical loop with a frequency shifter," *J. Lightwave Technol.*, vol. 15, pp. 2069–2075, Nov. 1997.

[6] A. Dandridge and A. B. Tveten, "Phase noise of single-mode diode lasers in interferometer systems," *Appl. Phys. Lett.*, vol. 39, pp. 530–532, Oct. 1981.
[7] B. Moslehi, "Noise power spectra of optical two-beam interferometers induced by the laser phase noise," *J. Lightwave Technol.*, vol. LT-4, pp. 1704–1709, Nov. 1986.
[8] J. L. Brooks, M. Tur, B. Y. Kim, K. A. Fesler, and H. J. Shaw, "Fiber-optics interferometric sensor arrays with freedom from source phase-induced noise," *Opt. Lett.*, vol. 11, pp. 473–475, July 1986.
[9] R. P. Morkel, R. I. Laming, and D. N. Payne, "Noise characteristics of high-power fiber superluminescent sources," *Electron. Lett.*, vol. 26, pp. 96–98, Jan. 1990.
[10] H. Hodara, "Statistics of thermal and laser radiation," *Proc. IEEE*, vol. 53, pp. 696–704, July 1965.
[11] L. Mandel, "Fluctuations of photon beams and their correlations," in *Proc. Phys. Soc.*, 1958, vol. 72, pp. 1037–1048.
[12] J. W. Goodman, *Statistical Optics*. New York: Wiley, 1985.
[13] K. P. Jackson, S. A. Newton, B. Moslehi, M. Tur, C. C. Cutler, J. W. Goodman, and H. J. Shaw, "Optical fiber delay-line signal processing," *IEEE Trans. Microwave Theory Tech.*, vol. MTT-33, pp. 193–208, Mar. 1985.
[14] M. Tur, E. Shafir, and K. Bløtekjaer, "Source-induced noise in optical systems driven by low-coherence sources," *J. Lightwave Technol.*, vol. 8, pp. 183–189, Feb. 1990.
[15] G. J. Pendock and D. D. Sampson, "Noise in coherence-multiplexed optical fiber systems," *Appl. Opt.*, vol. 36, pp. 9536–9540, Dec. 1997.
[16] A. Papoulis, *Probability, Random Variables, and Stochastic Processes*. New York: McGraw-Hill, 1991.
[17] R. Loudon, *The Quantum Theory of Light*. New York: Oxford Univ. Press, 1983.

Hyo Sang Kim, photograph and biography not available at the time of publication.

Ronald P. H. Haaksman, photograph and biography not available at the time of publication.

Trevor P. Newson, photograph and biography not available at the time of publication.

David J. Richardson, photograph and biography not available at the time of publication.